CHEMISTRY OF MATERIALS
Article

Chem. Mater. **2010,** *22,* 6673–6683 6673
DOI:10.1021/cm102705e

Enhanced Low-Temperature Proton Conduction in $Sr_{0.02}La_{0.98}NbO_{4-\delta}$ by Scheelite Phase Retention

A. D. Brandão,[†,‡] I. Antunes,[†] J. R. Frade,[†] J. Torre,[‡] V. V. Kharton,[†] and D. P. Fagg*[,‡]

[†]*Department of Ceramics and Glass Engineering, CICECO, University of Aveiro, 3810-193 Aveiro, Portugal, and* [‡]*Nanotechnology Research Division, Centre of Mechanical Technology and Automation, Department of Mechanical Engineering, University of Aveiro, 3810 193 Aveiro, Portugal*

Received September 20, 2010. Revised Manuscript Received October 22, 2010

The high-temperature scheelite phase of $Sr_{0.02}La_{0.98}NbO_4$ materials has been retained to room temperature via vanadium substitution for the $Sr_{0.02}La_{0.98}Nb_{1-x}V_xO_{4-\delta}$ compositional range of $0.25 \leq x \leq 0.325$. Such structural stabilization avoids the characteristic break in the thermal expansion coefficient (TEC) that may otherwise be deleterious for the application of $LaNbO_4$-based materials as proton-conducting electrolytes. The transport properties of composition $Sr_{0.02}La_{0.98}Nb_{0.7}V_{0.3}O_{4-\delta}$ have been extensively characterized. The composition offers pure proton conduction with higher conductivity than the base composition $Sr_{0.02}La_{0.98}NbO_{4-\delta}$ in the low-temperature range under wet oxidizing conditions. A wide ionic domain is observed, which increases as the temperature decreases. Suggested operational limits have been documented. Under dry oxidizing conditions, vanadium substitution is shown to suppress *p*-type conductivity, in comparison to the base composition $Sr_{0.02}La_{0.98}NbO_{4-\delta}$. In contrast, under wet conditions, $Sr_{0.02}La_{0.98}Nb_{0.7}V_{0.3}O_{4-\delta}$ is observed to be a pure proton conductor in oxygen and argon atmospheres at temperatures lower than ~700 °C. The total ionic conductivity equals that of the proton conductivity, within experimental error, suggesting negligible oxide-ion conduction in this material under these conditions.

1. Introduction

The most well-known ceramic-oxide proton-conducting protonic materials are perovskite oxides (ABO_3) with large basic A-cations (e.g., Ba, Sr) and tetravalent B cations (e.g., Zr, Ce). Unfortunately, most of these materials show poor tolerance to CO_2, rapidly decomposing to form carbonates (e.g., $BaCO_3$, $SrCO_3$) in the low- and intermediate-temperature ranges, because of the basicity of the alkali-earth A-cation.[1] This is a major problem when one considers using these materials in hydrocarbon and air environments in devices such as intermediate-temperature fuel cells or hydrogen separation membranes that offer in situ reforming. The recent discovery of alternative proton-conducting materials from structural families that offer high CO_2 tolerances, such as systems based on the fergusonite/scheelite $LaNbO_4$ structure types,[2−5] leaves a vast opportunity for scientific breakthrough, with respect to materials engineering, providing more-suitable materials for these devices.

To date, these phases have not received extensive characterization. Most work has been performed by Haugsrud et al.[2−4] and has shown that the highest proton conductivity is available in $LaNbO_4$ with minor A-site aliovalent substitutions. The essentially pure proton conduction in this class of materials has generated interest for applications such as hydrogen and humidity sensors at temperatures below ~700 °C, even though peak conductivity values remain an order of magnitude lower than those attainable in the perovskites.[2] Consequently, electrolyte thicknesses in the micrometer range are required, to achieve reasonable area-specific resistances in electrochemical devices.[2,6,7] In this respect, one major drawback may be the structural change of $LaNbO_4$ at ~600 °C, from the fergusonite structure to the scheelite polymorph, which is accompanied by a large change in thermal expansion; this feature is potentially problematic to the formation of mechanically stable films.[8] The fergusonite to scheelite phase transition is second order in nature,[9] and has even been shown to exhibit a broad temperature interval (450−750 °C) where both polymorphs can coexist by neutron and X-ray diffraction studies.[10,11] This is concerning, especially when one considers that the

*Author to whom correspondence should be addressed. Tel.: +351-234-370263. Fax: +351-234-425300. E-mail: duncan@ua.pt.

(1) Kreuer, K. D.; Adams, St.; Münch, W.; Fuchs, A.; Klock, U.; Maier, J. *Solid State Ionics* **2001**, *1−4*(145), 295.
(2) Haugsrud, R.; Norby, T. *Nat. Mater.* **2006**, *5*, 193.
(3) Haugsrud, R.; Norby, T. *Solid State Ionics* **2006**, *177*, 1129.
(4) Haugsrud, R.; Ballesteros, B.; Lira-Cantú, M.; Norby, T. *J. Electrochem. Soc.* **2006**, *153*, 187.
(5) Haugsrud, R.; Norby, T. *J. Am. Ceram. Soc.* **2007**, *90*, 1116.
(6) Fontaine, M.-L.; Larring, Y.; Haugsrud, R.; Norby, T.; Wiik, K.; Bredesen, R. *J. Power Sources* **2009**, *188*, 106.
(7) Lin, B.; Wang, S.; Liu, X.; Meng, G. *J. Alloys Compd.* **2009**, *478*, 355.
(8) Mokkelbost, T.; Lein, H. L.; Vullum, P. E.; Holmestad, R.; Grande, T.; Einarsrud, M.-A. *Ceram. Int.* **2009**, *35*, 2877.
(9) Jian, L.; Wayman, C. M. *J. Am. Ceram. Soc.* **1997**, *80*, 803.
(10) Malavasi, L.; Ritter, C.; Chiodelli, G. *J. Alloys Compd.* **2009**, *475*, 142.
(11) Aldred, A. T.; Nevitt, M. V.; Chan, S.-K. *J. Mater. Sci. Lett.* **1985**, *4*, 867.

Published on Web 12/01/2010

temperature interval of the phase transformation encompasses the desired operation temperature. Stubican et al.[12] noted that the onset temperature of the phase change increased as the ionic size of the rare-earth dopant decreased and was higher for the rare-earth tantalates than for the corresponding niobates. Based on these observations, previous authors have suggested a potential solution to the phase change problem that involves the retention of the low-temperature fergusonite polymorph to higher temperature either via the partial substitution of Nb for Ta or the reduction in the ionic size of the rare-earth element.[2,13] In this respect, one should be aware that the tantalate-based fergusonite compositions offer substantially lower proton conductivities than their niobate counterparts[2,5] and that a major reduction in proton conduction results from reductions in the size of the rare-earth cation.[2] Hence, both of the methods that have currently been suggested to maintain phase stability by retention of the fergusonite phase will negatively influence the resultant level of proton conductivity. Furthermore, it is important to note that it is the high-temperature scheelite phase, which offers the lower activation energy for proton conduction, in comparison to a rapid decay of conductivity with decreasing temperature for the fergusonite polymorph.[3] Hence, the objective of the current work is to investigate the inverse solution whereby the high-temperature scheelite phase is stabilized down to room temperature (avoiding phase changes and potential mechanical failure) while potentially retaining high levels of proton conductivity to lower temperatures, due to a lower activation energy.

In the 1980s, Bastide summarized the phase transitions of ABX_4 compounds, with respect to their cation−anion radii ratio coordinates (r_A/r_x, r_B/r_x), as a function of their coordination chemistry,[14] and this work has been recently updated by Manjón et al.[15] A simplified version of Manjón's diagram is shown in Figure 1, highlighting the regions of interest for the current materials. Figure 1 concludes that retention of the high-temperature scheelite polymorph to low temperatures is most likely induced by reduction of the size of the B-site cation. In agreement, Brik et al.[16] noted that the scheelite polymorph of $LaNbO_4$ can be retained to room temperature by the B-site substitution of niobium with smaller vanadium cations. Therefore, the current work assesses the impact of scheelite phase retention on the levels of proton and electron conduction in the $Sr_{0.02}La_{0.98}Nb_{0.7}V_{0.3}O_{4-\delta}$ material in the search for potential components for intermediate temperature fuel cells, electrolyzers, and separation membranes that can operate in hydrocarbon atmospheres. Because potential B-site substitutions have not previously been attempted in this class of material, nor methods

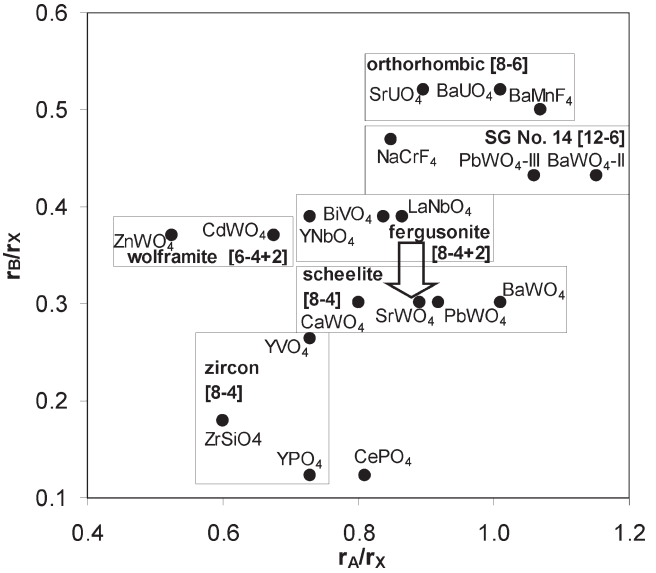

Figure 1. Simplified version of Manjón's diagram showing the phase transitions of ABX_4 compounds, with respect to their cation−anion radii ratio coordinates (r_A/r_x, r_B/r_x), as a function of their coordination chemistry.[15]

of scheelite phase retention, in the pursuit of novel proton-conducting materials, this preliminary work is expected to encourage many further studies, especially because a wide range of further potential B-site dopant cations, both aliovalent and isovalent, can be envisaged.

2. Experimental Section

2.1. Sample Preparation and Materials Properties. Powders of $Sr_{0.02}La_{0.98}Nb_{1-x}V_xO_{4-\delta}$ were prepared via solid-state synthesis, starting from stoichometric mixtures of $SrCO_3$, La_2O_3, Nb_2O_5, and V_2O_5, for values of x = 0.15, 0.20, 0.25, 0.30, 0.35, 0.40, 0.45, and 0.50. Stoichiometric amounts of the reagents were intimately mixed in a mortar and pestle under acetone, uniaxially dry-pressed into pellets at a pressure of 30 MPa, and fired at 1300 °C for 10 h. Phase analysis was performed by X-ray diffraction (XRD), on crushed powders using a Rigaku Geigerflex diffractometer (Cu Kα radiation), (15°−115° 2θ, step 0.02, 6 s/step). Unit-cell parameters were determined from the diffraction data using Fullprof software.[17]

Stability in flowing CO_2 was assessed by thermogravimetric analysis, using a Setaram Model SetSys 16/18 instrument. Stability was further assessed by post-mortem examination by XRD of samples annealed for 5 h in dry hydrogen atmospheres at 900 °C. For electrical and thermal characterization, further processing was required to achieve sample densities exceeding 90% of the theoretical density. Samples of composition $Sr_{0.02}La_{0.98}Nb_{0.7}V_{0.3}O_{4-\delta}$ were prepared as previously documented. These samples were broken into powders and lightly milled in ZrO_2 vials with ZrO_2 balls for 30 min, at 100 rpm, in a planetary ball mill (Retsch, Model PM200). The powder was then sieved (20 μm mesh) and uniaxially pressed into pellets at 30 MPa, followed by isostatic pressing for 15 min at 230 MPa, and then was refired at 1400 °C for 10 h, using sacrificial powder of the same composition. The continued absence of secondary phases was confirmed by XRD and scanning electron microscopy (SEM). Average grain sizes were calculated to be in the range

(12) Stubican, V. S. *J. Am. Ceram. Soc.* **1964**, *47*, 55.
(13) Vullum, F.; Nitsche, F.; Selbach, S. M.; Grande, T. *Solid State Chem.* **2008**, *181*, 2580.
(14) Bastide, J. P. *J. Solid State Chem.* **1987**, *71*, 115.
(15) Manjón, F. J.; Errandonea, D.; López-Solano, J.; Rodríguez-Hernández, P.; Radescu, S.; Mujica, A.; Muñoz, A.; Garro, N.; Pellicer-Porres, J.; Segura, A.; Ferrer-Roca, Ch.; Kumar, R. S.; Tschauner, O.; Aquilanti, G. *Phys. Status Solidi B* **2007**, *244*, 295.
(16) Brik, F.; Enjalbert, R.; Galy, J. *Mater. Res. Bull.* **1994**, *29*, 15.
(17) Rodríguez-Carvajal, J. *Physica B* **1993**, *192*, 55.

of 3−10 μm for both samples, from SEM images, using the image processing program ImageJ 1.37v software (Wayne Rasband, National Institutes of Health (NIH), USA). Thermal expansion behavior was followed using a Linseis dilatometer on rectangular green compacts (1.3 cm × 0.5 cm × 0.5 cm) with a constant heating and cooling rate of 10 °C/min.

2.2. Coulometric Titration and Electrical Measurements. Data on oxygen stoichiometry for the scheelite composition $Sr_{0.02}La_{0.98}Nb_{0.7}V_{0.3}O_{4-\delta}$ were obtained by the coulometric titration technique. Coulometric titration was performed as a function of oxygen partial pressure in potentiostatic mode, as described elsewhere.[18] Variations in oxygen content were measured with respect to a reference point of atmospheric oxygen pressure. The potentiostatic mode has the benefit that the unavoidable leakage current (I_{leak}) is given by the value to which the current decays after a potentiostatic step. The change in sample oxygen nonstoichiometry ($\Delta\delta$) is given by the integration of the current (I) over time (t), through the yttria-stabilized zirconia (YSZ) solid electrolyte electrochemical cell:

$$\Delta\delta = \frac{M}{m_{sample}} \int_{t=0}^{t=\infty} \frac{I(t) - I_{leak}}{2F} \, dt \quad (1)$$

where M is the molar mass, m_{sample} the mass of the sample, and F the Faraday constant.

Total conductivity in a dry ($p(H_2O) \approx 1 \times 10^{-5}$ atm) atmosphere was measured on dense bars, with dimensions of ~2 mm × 4 mm × 12 mm, with painted porous platinum electrodes, using the four-point DC method in a controlled atmosphere device, as described in detail elsewhere.[19,20]

Impedance spectroscopy was performed using an Electrochemie-Autolab PGSTAT302N analyzer, with a frequency range of 1 MHz to 0.01 Hz and an amplitude of 50 mV, on dense pellets with dimensions of ~3 mm × 8 mm (length × diameter), painted with two porous platinum electrodes, in an isolated chamber under both wet and dry nitrogen and oxygen atmospheres, at a flow rate of 50 mL/min. The impedance data were deconvoluted to obtain contributions ascribed to the bulk, grain boundaries, and external interfaces, as confirmed by typical capacitance values in the ranges of 10−20 pF/cm^2, ~1 nF/cm^2, and ~1 μF/cm^2, respectively. Measurements were made at 50 °C intervals in the direction of decreasing temperature. Stability was confirmed by performing repeated impedance measurements at each temperature. Humidification was obtained by bubbling gases through water, followed by a saturated KCl solution in contact with solid KCl, producing ~86% relative humidity at room temperature. Drying was performed by passing the gas through a Varian moisture gas clean filter.

The total conductivity of the grain boundaries in series with the bulk material can be estimated using the brick-layer model, as described in ref 21:

$$\sigma_{gb} = \frac{L}{A}\left(\frac{C_{bulk}}{C_{gb}}\right)\frac{1}{R_{gb}} \quad (2)$$

where A is the cross-sectional area, L the length, R_{gb} the grain-boundary resistance extracted from the impedance spectra, and C_{bulk} and C_{gb} are the bulk and boundary capacitances, respectively.

2.3. Ion Transport Number Determination. The proton and oxygen ion transference numbers were determined by measuring the electromotive force (EMF) of water-vapor and oxygen concentration cells. For a galvanic cell exposed to a gradient in chemical potential of an ionic species i, the open-circuit potential (OPC) can be defined as[22]

$$E_{OPC} = -\frac{1}{F}\int_{\mu_1}^{\mu_2} \frac{t_i}{nF} \, d\mu_i \quad (3)$$

where t_i is the transport number for species i, n is the number of electrons transferred, and μ_2 and μ_1 are the chemical potentials of species i at the reversible electrodes. For a gradient of gaseous species, this equation can be written as

$$E_{OPC} = -\frac{RT}{F}\int_{p_1}^{p_2} \frac{t_i}{nF} \, d \ln p_i \quad (4)$$

where R is the universal gas constant, T is the temperature, and p_1 and p_2 are the respective partial pressures of the electrochemically active gas in the inner and outer compartments. In a cell where simultaneous proton or oxide-ion conduction may occur, one must take into account the relationship between oxygen, hydrogen, and water vapor:

$$\frac{1}{2}O_2 + 2e^- \leftrightarrow O^{2-} \quad (5)$$

$$H_2O \leftrightarrow 2H^+ + \frac{1}{2}O_2 + 2e^- \quad (6)$$

or corresponding expressions for materials with coexisting oxygen ions, protons, and electron holes. The open-circuit voltage is then related to the transport number of protons (t_H) and oxygen ions (or oxygen vacancies) (t_O), as described by[23]

$$E_{OPC} = \frac{RT}{4F}(t_H + t_O)\ln\left(\frac{p^2(O_2)}{p^1(O_2)}\right) - \frac{RT}{2F}(t_H)\ln\left(\frac{p^2(H_2O)}{p^1(H_2O)}\right) \quad (7)$$

The experimental setup is shown in Figure 2, while the method follows that described by Sutija et al.[24] At the first stage, equal partial pressures of oxygen in inert gas were flowed to both cell compartments while a water vapor concentration gradient was set up across the cell. This allowed t_H to be calculated in wet oxidizing environments for conditions when eq 7 reduces to

$$E_{OPC} \approx -\frac{RT}{2F}(t_H)\ln\left(\frac{p^2(H_2O)}{p^1(H_2O)}\right) \quad (8)$$

An in-built oxygen sensor (see Figure 2) confirmed the absence of an oxygen partial pressure gradient. Conversely, a gradient in oxygen partial pressure across the cell under a zero-water-vapor concentration gradient allowed calculation of the total ionic transport number ($t_O + t_H$). In these two experiments, the average conditions were arranged to be equal, so that the average transport numbers remained constant.

(18) Lankhorst, M. H. R.; Bouwmeester, H. J. M. *J. Electrochem. Soc.* **1997**, *144*, 1268.
(19) Fagg, D. P.; Frade, J. R.; Kharton, V. V.; Marozau, I. P. *J. Solid State Chem.* **2006**, *179*, 1469.
(20) Leonidov, I. A.; Kozhevnikov, V. L.; Mitberg, E. B.; Patrakeev, M. V.; Kharton, V. V.; Marques, F. M. B. *J. Mater. Chem.* **2001**, *11*, 1202.
(21) Haile, S. M.; Staneff, G.; Ryuj, K. H. *Mater. Sci.* **2001**, *36*, 1149.
(22) Wagner, C. *Z. Phys. Chem., Abt. B* **1933**, *25*, 21.
(23) Frade, J. R. *Solid State Ionics* **1995**, *78*, 87.
(24) Sutija, D. P.; Norby, T.; Björnbom, P. *Solid State Ionics* **1995**, *77*, 167.

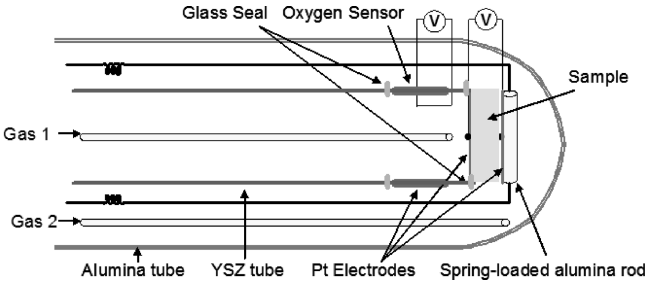

Figure 2. Schematic of experimental setup for transport number determination by EMF measurements. The key part is represented by a disk with two porous platinum electrodes, hermetically sealed onto a YSZ tube with a sensor. The tube is inserted into a closed chamber; two flowing gas mixtures are continuously supplied onto the electrodes.

Solving these E_{OPC} expressions should give the transport numbers of protons (t_H), oxide ions (t_O), and electrons ($t_e = 1 - t_O - t_H$). However, a simple interpretation based on eq 7 often leads to incoherent values for these parameters. For example, slight temperature gradients might yield a significant thermovoltage contribution. Thus, OCV measurements were corrected for thermovoltages by inverting the gas flow (i.e., by reversal of the chemical potential gradient). The offset voltage was then eliminated by subtracting and averaging the voltages measured under forward and reverse conditions:

$$E_{OCV} = \frac{E_{forward} - E_{reverse}}{2} \quad (9)$$

Errors related to the polarization resistance of the electrodes were taken into account via a modification of the external load method, as described in the literature.[25,26]

Activation energy (E_a) values for the partial conductivities were calculated using the standard Arrhenius equation,

$$\sigma = \frac{A_0}{T}\exp\left(-\frac{E_a}{RT}\right) \quad (10)$$

where A_0 is the pre-exponential factor.

3. Results and Discussion

3.1. Structural Characterization. The XRD patterns of $La_{0.98}Sr_{0.02}Nb_{1-x}V_xO_{4-\delta}$ materials for values of x = 0.15, 0.20, 0.25, 0.30, 0.35, 0.40, 0.45, and 0.50 are shown in Figure 3. In the current materials, a small concentration of strontium must be substituted on the La site to create oxygen vacancies that can react with water vapor to form protons localized on O^{2-} ions.[2−5] In Kröger−Vink notation, and, upon assuming that charge compensation in a generic fergusonite material $Sr_zLa_{1-z}Nb_{1-x}V_xO_{4-\delta}$ is exclusively determined by ionic defects, this process can be described as

$$zSrO + (1-z)LaO_{1.5} + (1-x)NbO_{2.5} + xVO_{2.5} \rightarrow zSr_{La}' + (1-z)La_{La}^{\times} + (1-x)Nb_{Nb}^{\times} + xV_{Nb}^{\times} + 0.5zV_O^{\bullet\bullet} + (4-0.5z)O_O^{\times} \quad (11)$$

At low vanadium concentrations, the XRD patterns of $Sr_{0.02}La_{0.98}Nb_{1-x}V_xO_{4-\delta}$ materials can be properly refined using the space group $I2/a$ of the low-temperature fergusonite-type monoclinic form of $LaNbO_4$.[10,27] As the value of x increases, the high-temperature scheelite tetragonal form becomes stabilized to room temperature and, correspondingly the XRD patterns of the scheelite compositions can be adequately refined using the space group $I4_1/a$.[9,27,28] A plot of the composition variation of the lattice parameters is given in Figure 4. One observes coincidence of the monoclinic parameters a and c with increasing vanadium concentration, until the scheelite phase forms. From consideration of Vegard's law, the lower limit of the pure scheelite phase can be placed at composition $x = 0.25$, whereas for values of $x \geq 0.35$, a two-phase equilibrium is observed between the scheelite phase of maximum vanadium content and the monoclinic monazite-type structure of $LaVO_4$, in accordance with the lever rule. These observations imply contraction in the extent of scheelite solid solution for strontium-containing compositions, when compared to the compositional limits reported by Aldred for strontium-free compositions: $0.2 < x < 0.37$.[29] A further point of interest is the discontinuous change in lattice volume with increasing vanadium content. Within the fergusonite phase boundaries, the lattice volume increases as the vanadium content increases, by expansion of the b-axis, whereas the inverse trend occurs within the scheelite phase limits. Such discontinuous changes in lattice volume have also been reported to occur in other $ANb_{1-x}V_xO_4$ compounds (e.g., where A = La, Ce, and Nd)[30] and are consistent with differences between the ionic radii of Nb^{5+} and V^{5+} in 4-fold coordination in the scheelite structure.

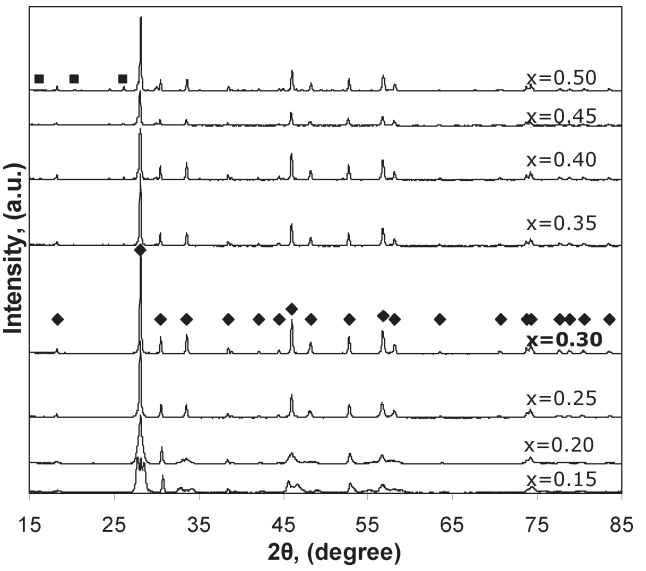

Figure 3. XRD patterns of $Sr_{0.02}La_{0.98}Nb_{1-x}V_xO_{4-\delta}$ materials for values of x = 0.15, 0.20, 0.25, 0.30, 0.35, 0.40, 0.45, and 0.50. The markers identify the $LaNb_{0.7}V_{0.3}O_{4-\delta}$ scheelite phase (◆) and the $LaVO_4$ monazite phase (■).

3.2. Carbon Tolerance and Thermal Expansion. Figure 5 demonstrates carbon tolerances of $Sr_{0.02}La_{0.98}Nb_{0.7}V_{0.3}O_{4-\delta}$

(25) Bentzer, H. K.; Bonanos, N.; Phair, J. W. *Solid State Ionics* **2010**, *181*, 249.
(26) Frade, J. R.; Kharton, V. V.; Yaremchenko, A. A.; Tsipis, E. V. *J. Solid State Electrochem.* **2006**, *10*, 96.
(27) Packer, R. J.; Stuart, P. A.; Skinner, S. J. *J. Solid State Chem.* **2008**, *181*, 1445.
(28) David, W. I. F. *Mater. Res. Bull.* **1983**, *18*, 749.
(29) Aldred, A. T. *Mater. Lett.* **1983**, *1*, 197.
(30) Aldred, A. T. *J. Solid State Chem.* **1985**, *59*, 95.

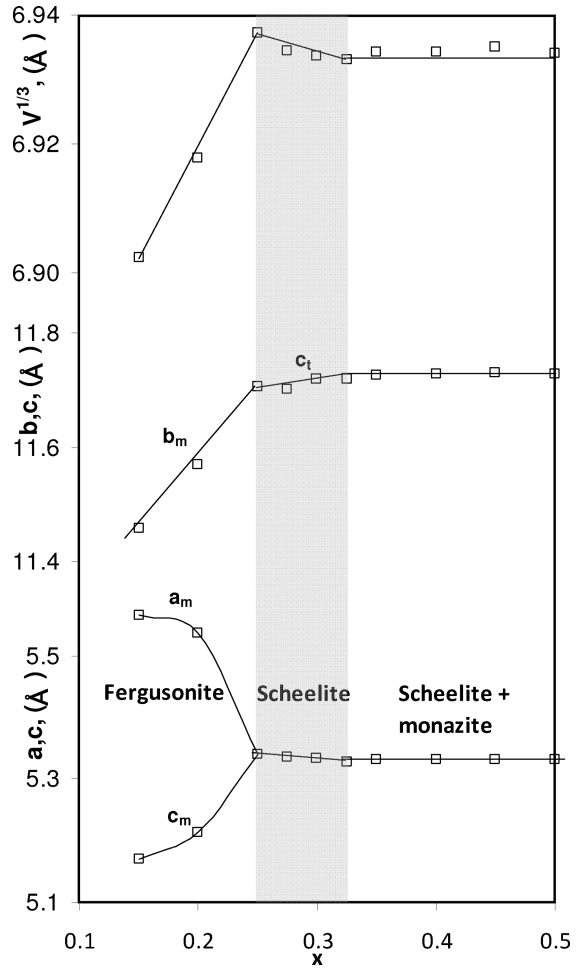

Figure 4. Compositional variation of lattice parameters and cell volume in $Sr_{0.02}La_{0.98}Nb_{1-x}V_xO_{4-\delta}$ materials. Lines are present for visual guidance. The shaded area represents the extent of the pure scheelite phase.

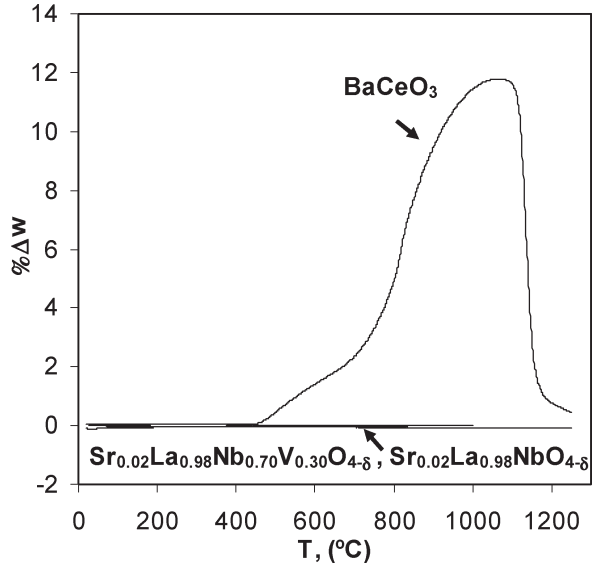

Figure 5. Carbon tolerances of compositions $Sr_{0.02}La_{0.98}Nb_{0.7}V_{0.3}O_{4-\delta}$ and $Sr_{0.02}La_{0.98}NbO_{4-\delta}$, compared to a typical barium-containing perovskite proton-conducting electrolyte material ($BaCeO_3$) in flowing dry CO_2.

and $Sr_{0.02}La_{0.98}NbO_{4-\delta}$ in flowing dry CO_2. For the vanadium-containing composition, this tolerance is much better than that of typical barium-containing perovskite proton-conducting electrolyte materials based on $BaCeO_3$.[31] This observation reinforces the potential use of this novel family of materials in hydrocarbon environments. Figure 6 compares the thermal expansion behavior of $Sr_{0.02}La_{0.98}Nb_{0.7}V_{0.3}O_{4-\delta}$ with that of $Sr_{0.02}La_{0.98}NbO_{4-\delta}$. The thermal expansion behavior of the vanadium-free composition shows a clear discontinuity at ~550 °C, which is characteristic of the second-order fergusonite-to-scheelite phase transformation.[9] The respective thermal expansion coefficients (TECs) for the two ranges are calculated to be 20×10^{-6} K^{-1} and 8×10^{-6} K^{-1}. These values are in agreement with the literature.[8] In contrast, the composition $Sr_{0.02}La_{0.98}Nb_{0.7}V_{0.3}O_{4-\delta}$ maintains a constant TEC (8×10^{-6} K^{-1}) throughout the temperature range. Notice that this TEC is essentially equal to the high-temperature TEC of $Sr_{0.02}La_{0.98}NbO_{4-\delta}$ (corresponding to the scheelite phase) and, furthermore, is of the order of typical SOFC oxide-ion conducting electrolyte materials (e.g., YSZ). Therefore, the incorporation of vanadium and retention of the scheelite phase to room temperature produces a material that offers a stable TEC.

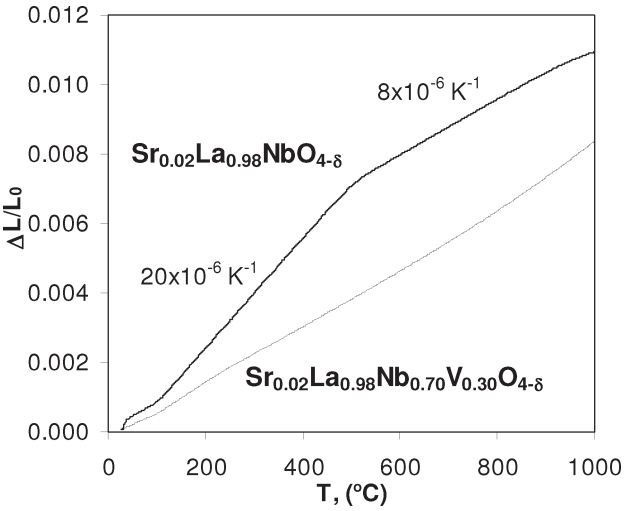

Figure 6. Thermal expansion behavior of composition $Sr_{0.02}La_{0.98}Nb_{0.7}V_{0.3}O_{4-\delta}$, compared to that of $Sr_{0.02}La_{0.98}NbO_{4-\delta}$.

3.3. Coulometric Titration and Stability under Reducing Conditions. Coulometric titration results for $Sr_{0.02}La_{0.98}Nb_{0.7}V_{0.3}O_{4-\delta}$ are presented in Figure 7, in the form of a $p(O_2)-T-\Delta\delta$ diagram, with respect to a reference point of air. The $p(O_2)$ dependence of oxygen nonstoichiometry exhibits four distinct trends with decreasing oxygen partial pressure. At high $p(O_2)$, oxygen nonstoichiometry remains constant with decreasing oxygen partial pressure. This is followed, at intermediate $p(O_2)$ values, by small increases in oxygen nonstoichiometry, until a narrow $p(O_2)$ range is attained, where rapid losses of oxygen occur. Finally, at the lowest $p(O_2)$ values, further decreases in $p(O_2)$ induce monotonous increases in oxygen stoichiometry with weak dependence. The oxygen partial pressures that correspond to the onset of the second, third, and fourth stages are shifted to continuously lower values with decreasing study

(31) Zakowsky, N.; Williamson, S.; Irvine, J. T. S. *Solid State Ionics* **2005**, *176*, 3019.

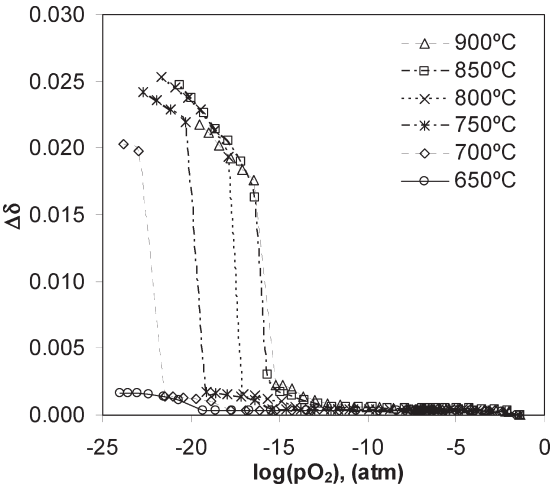

Figure 7. Coulometric titration results for composition $Sr_{0.02}La_{0.98}Nb_{0.7}V_{0.3}O_{4-\delta}$ in the form of a $p(O_2)-T-\Delta\delta$ diagram, with respect to a reference point of air.

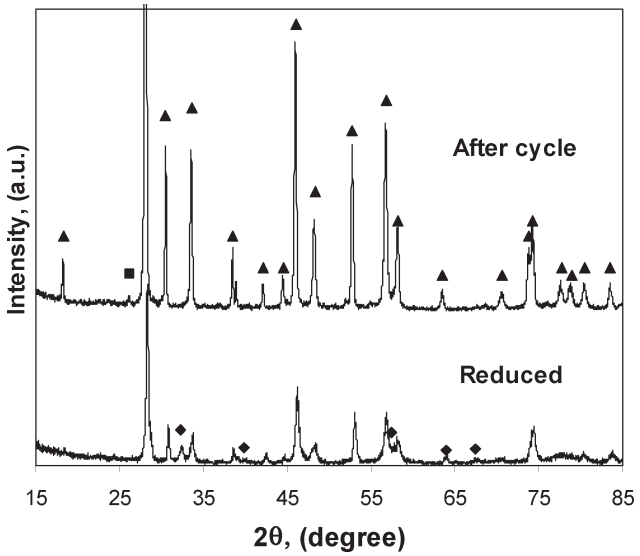

Figure 8. XRD of a powder sample of $Sr_{0.02}La_{0.98}Nb_{0.7}V_{0.3}O_{4-\delta}$ calcined at 900 °C for 5 h and cooled under flowing 10% H_2/N_2 atmosphere, and again after reoxidation in air at 900 °C. The markers identify the $LaNb_{0.7}V_{0.3}O_{4-\delta}$ scheelite phase (▲), the $LaVO_3$ phase (◆), and the $LaVO_4$ phase (■).

temperatures, until, at the lowest temperature analyzed (650 °C), the third and fourth stages are no longer observable within the measured $p(O_2)$ range.

To assist in the understanding, XRD data were collected on a powder sample of $Sr_{0.02}La_{0.98}Nb_{0.7}V_{0.3}O_{4-\delta}$ calcined at 900 °C for 5 h and cooled under flowing 10% H_2/N_2 atmosphere, and again after reoxidation in air at 900 °C (see Figure 8). The XRD pattern of the reduced sample reveals slight decomposition of the main scheelite phase with formation of the perovskite $LaVO_3$. However, note that the majority of the vanadium must remain in the main phase upon reduction, to retain the scheelite structure. Upon reoxidation, a fraction of this impurity phase is unable to reintegrate into the main phase, but instead forms a minor impurity of segregated monazite, $LaVO_4$.

Yokokawa et al.[32] and, more recently, Shah et al.[33] have documented the redox properties of a range of vanadia-based, ABO_4 mixed oxides. Interestingly, the monazite materials $CeVO_4$ and $LaVO_4$ were shown to exhibit very similar reduction properties to each other, directly reducing from $V^{5+} \rightarrow V^{3+}$ in one step at very low oxygen partial pressures (e.g., 10^{-18} atm at 700 °C). In contrast, the binary oxide V_2O_5 undergoes a two-step reduction mechanism, between $V^{5+} \rightarrow V^{4+}$ under more-oxidizing conditions (10^{-6} atm. at 600 °C), followed by $V^{4+} \rightarrow V^{3+}$ under more-reducing conditions (10^{-18} atm at 600 °C). Such stabilization of vanadium in the 5+ oxidation state was suggested to be due to the absence of V−O−V bonds in the monazite structure; hence, reduction of these materials requires the energetically unfavorable removal of oxygen from either a La−O−V or Ce−O−V lattice site. In this respect, one notes that the scheelite material, $Sr_{0.02}La_{0.98}Nb_{0.7}V_{0.3}O_{4-\delta}$, possesses a very similar crystallographic structure, involving B-site atoms in the center of isolated tetrahedra of O atoms. Note that V^{4+} and V^{3+} ions are both significantly larger than V^{5+} and unlikely to assume the required 4-coordination. In agreement with this analogy, one observes that the reduction behavior of $Sr_{0.02}La_{0.98}Nb_{0.7}V_{0.3}O_{4-\delta}$ mirrors that of the monazite materials, with reduction of vanadium occurring only under comparatively very low oxygen partial pressures. The $p(O_2)$ value that corresponds to the onset of second-stage reduction in $Sr_{0.02}La_{0.98}Nb_{0.7}V_{0.3}O_{4-\delta}$ is similar to that noted for the $V^{5+} \rightarrow V^{3+}$ reduction in $LaVO_4$ by Shah et al.[33] Hence, it is hypothesized that second-stage reduction corresponds to the onset of $V^{5+} \rightarrow V^{3+}$ reduction in the bulk scheelite phase, followed by third-stage reduction, with rapid oxygen loss, associated with partial phase decomposition and the formation of trace amounts of $LaVO_3$. Upon the assumption of direct reduction of $V^{5+} \rightarrow V^{3+}$, second-phase reduction corresponds to ~1% of the vanadium present, while third-phase reduction corresponds to ~10% of the vanadium present. These low values of vanadium reduction support the conclusion that the majority of the vanadium must remain both unreduced and in the bulk material to continue to stabilize the scheelite phase.

The objective of this work was to design materials for use in devices such as fuel cells that function in hydrocarbon environments. Hence, Figure 9 compares the stability limits of second-stage and third-stage reduction in $Sr_{0.02}La_{0.98}Nb_{0.7}V_{0.3}O_{4-\delta}$, as identified by coulometric titration, to typical conditions expected upon operation in two typical biogas fuel mixtures: 75% CH_4:25% CO_2 and 50% CH_4:50% CO_2, relating to the products of anaerobic digestion of agricultural waste and landfill, respectively.[34] Corresponding $p(O_2)$ values were predicted by thermodynamic considerations.[35] In addition,

(32) Yokokawa, H.; Sakai, N.; Kawada, T.; Dokiya, M. *J. Am. Ceram. Soc.* **1990**, *73*, 649.
(33) Shah, P. R.; Khader, M. M.; Vohs, J. M.; Gorte, R. J. *J. Phys. Chem. C* **2008**, *112*, 2613.
(34) Deublein, D., Steinhauser, A. *Biogas from Waste and Renewable Sources*; Wiley−VCH Verlag GmbH & Co., KGaA: Weinheim, Germany, 2008.
(35) Frade, J. R.; Kharton, V. V.; Yaremchenko, A.; Naumovich, E. *J. Power Sources* **2004**, *130*, 77.

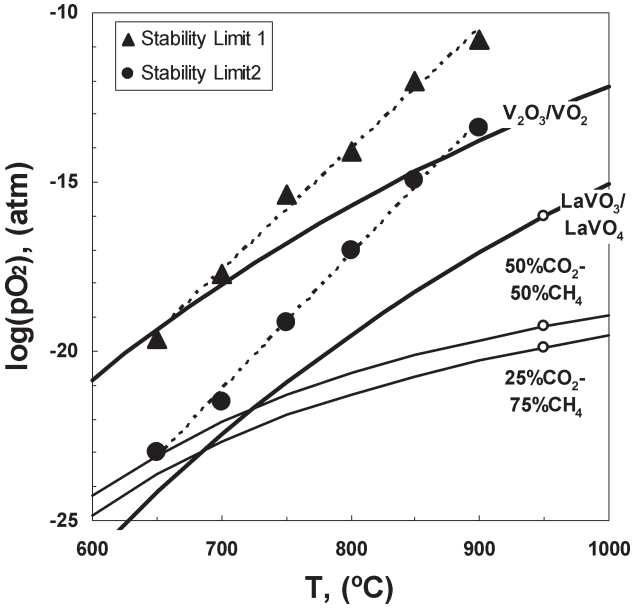

Figure 9. Comparison of stability limits of second-stage and third-stage reduction in $Sr_{0.02}La_{0.98}Nb_{0.7}V_{0.3}O_{4-\delta}$, as identified by coulometric titration, with the $p(O_2)$ conditions expected for two typical biogas fuel mixtures (75% CH_4:25% CO_2 and 50% CH_4:50% CO_2, predicted by thermodynamic considerations).

Figure 9 shows predictions of redox equilibrium conditions for the relevant vanadium oxide pair V_2O_3/VO_2 and for lanthanum vanadates $LaVO_3/LaVO_4$, based on ref 32. One observes that third-stage reduction, corresponding to structural stability, will only be attained for the composition $Sr_{0.02}La_{0.98}Nb_{0.7}V_{0.3}O_{4-\delta}$ in these biogas-type mixtures, at temperatures approaching 600 °C. Nevertheless, in a fuel cell scenario, the electrolyte will be subjected to an oxygen partial pressure gradient with the cathode side under oxidizing conditions, thus assisting the phase stability of the bulk electrolyte material to higher temperatures, except possibly for a surface layer in contact with the fuel atmosphere. Note also that slight reduction on the anode side may actually be advantageous, since the onset of electronic conduction at the surface of electrolyte materials has been shown to reduce overpotential losses, because of the extension of electrocatalytically active sites.[36,37]

3.4. Total Conductivity, as a Function of Oxygen Partial Pressure in dry conditions. Figure 10 shows the oxygen partial pressure dependence of the total DC conductivity of $Sr_{0.02}La_{0.98}Nb_{0.7}V_{0.3}O_{4-\delta}$ measured under dry conditions ($p(H_2O) \approx 1 \times 10^{-5}$ atm). Care was taken not to exceed the low $p(O_2)$ values that correspond to the structural stability limits, identified by the coulometric titration results in section 3.3. At high temperatures, the dependence of conductivity on the oxygen pressure changes slope with changing $p(O_2)$; from negative under reducing conditions to positive under more-oxidizing conditions. Under dry oxidizing conditions, this trend mirrors the reported

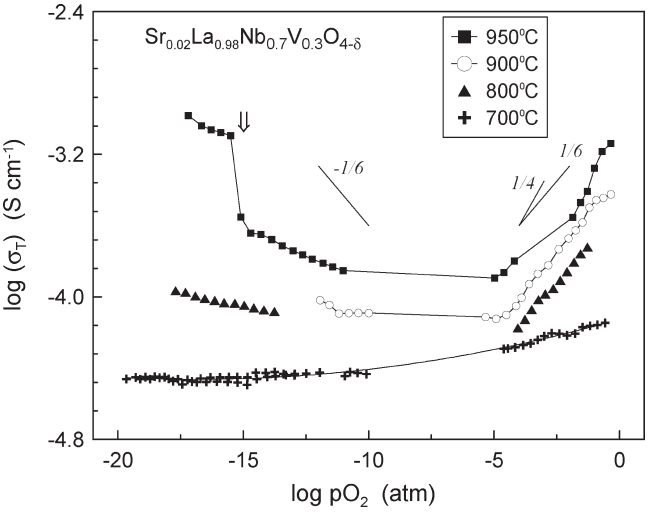

Figure 10. Oxygen partial pressure dependence of the total DC conductivity of $Sr_{0.02}La_{0.98}Nb_{0.7}V_{0.3}O_{4-\delta}$ measured under dry conditions ($p(H_2O) \approx 10^{-5}$ atm).

p-type electronic behavior of the base material: acceptor-doped $LaNbO_4$, as described by Norby et al.[3] The equilibrium of oxygen vacancies and electron holes with the surrounding atmosphere can be described by the equation

$$V_O^{\bullet\bullet} + \frac{1}{2}O_2(g) \overset{K_{ox}}{\Leftrightarrow} O_O^{\times} + 2h^{\bullet} \quad (12)$$

with a mass action constant described by

$$K_{ox} = \frac{[O_O^{\times}]p^2}{[V_O^{\bullet\bullet}]p(O_2)^{1/2}} \quad (13)$$

This process may compete with the incorporation of protons by water vapor uptake as follows:

$$O_O^{\times} + V_O^{\bullet\bullet} + H_2O(g) \overset{K}{\Leftrightarrow} 2OH_O^{\bullet} \quad (14)$$

with a mass action constant described as

$$K = \frac{[OH_O^{\bullet}]^2}{[V_O^{\bullet\bullet}][O_O^{\times}]p(H_2O)} \quad (15)$$

Under oxidizing conditions, one can neglect the concentration of electrons and, thus, description of the defect chemistry is completed by the addition of the electroneutrality condition:

$$p + [OH_O^{\bullet}] + 2[V_O^{\bullet\bullet}] \approx [Sr_{La}'] \quad (16)$$

Because the level of acceptor doping is low,

$$h^{\bullet} + [OH_O^{\bullet}] + [V_O^{\bullet\bullet}] \ll [O_O^{\times}] \approx [O] \quad (17)$$

Hence, upon combining eqs 13, 15, and 16, one obtains

$$(K_{ox}^{1/2}[O]^{-1/2}p(O_2)^{1/4} + K^{1/2}[O]^{1/2}p(H_2O)^{1/2})[V_O^{\bullet\bullet}]^{1/2} + 2[V_O^{\bullet\bullet}] \approx [Sr_{La}'] \quad (18)$$

(36) Fagg, D. P.; Kharton, V. V.; Frade, J. R. *J. Solid State Electrochem.* **2004**, *8*, 618.
(37) Bohac, P.; Orliukas, A.; Gauckler, L. J. In *Proceedings of the International Conference, "Electroceramics IV"*, Vol. *2*; Waser, R., Ed.; Augustinus Buchhandlung: Aachen, Germany, 1995; p 771.

and, thus,

$$[V_O^{\bullet\bullet}] = 0.5[Sr_{La}']F_{wc}[(1+F_{wc}^{-1})^{1/2}-1]^2 \quad (19)$$

where

$$F_{wc} = [\left(\frac{K_{ox}}{8[O][Sr_{La}']}\right)^{1/2} p(O_2)^{1/4} + \left(\frac{K[O]}{8[Sr_{La}']}\right)^{1/2} p(H_2O)^{1/2}]^2 \quad (20)$$

is a function of relative contributions of working conditions, including the dependence on the partial pressures of oxygen and water vapor and also the temperature dependence of mass action constants K_{ox} and K. Upon combining eq 19 with eqs 13 and 15, one also obtains

$$p = \left(\frac{[Sr_{La}']K_{ox}F_{wc}}{2[O]}\right)^{1/2} p(O_2)^{1/4}[(F_{wc}{}^{-1}+1)^{1/2}-1] \quad (21)$$

$$[OH_O^{\bullet}] = \left(\frac{K[O][Sr_{La}']F_{wc}}{2}\right)^{1/2} (p(H_2O))^{1/2}[(F_{wc}{}^{-1}+1)^{1/2}-1] \quad (22)$$

Under very dry oxidizing conditions, one can assume $K_{ox}{}^{1/2}p(O_2)^{1/4} \gg K^{1/2}[O]p(H_2O)^{1/2}$, yielding the following:

$$p = \frac{K_{ox}p(O_2)^{1/2}}{4[O]}\left[\left(1+\frac{8[Sr_{La}'][O]}{K_{ox}p(O_2)^{1/2}}\right)^{1/2}-1\right] \quad (23)$$

with limiting regimes for weakly oxidizing conditions (eq 24) and strongly oxidizing conditions (eq 25):

$$p \approx (0.5K_{ox}\frac{[Sr_{La}']}{[O]})^{1/2}p(O_2)^{1/4} \quad (24)$$

$$p \approx [Sr_{La}'] \quad (25)$$

Therefore, the dependence of $p(O_2)^{1/4}$ for *p*-type electronic conductivity is in agreement with the observed results of Figure 10 at high temperatures.

The negative conductivity dependence on $p(O_2)$ under reducing conditions suggests *n*-type conductivity behavior. The base acceptor-doped $LaNbO_4$ composition has also been reported to show *n*-type electronic conductivity at very high temperatures,[3] most likely because of oxygen exchange combined with intrinsic ionization. Upon combining the mass action constant $K_i = np$ with eq 24, one should expect the $p(O_2)^{-1/4}$ for *n*-type electronic charge carriers.

$$n \approx K_i(0.5K_{ox}\frac{[Sr_{La}']}{[O]})^{-1/2}p(O_2)^{-1/4} \quad (26)$$

However, for the vanadium-containing analogue, $Sr_{0.02}La_{0.98}Nb_{0.7}V_{0.3}O_{4-\delta}$, the coulometric titration measurements (section 3.3) concluded that oxygen loss at intermediate partial pressures (second-stage reduction) could be related to direct $V^{5+} \rightarrow V^{3+}$ reduction. The correlation of the results of Figure 10 to second-stage reduction was confirmed at 950 °C by exceeding the structural stability limit. Because this leads to segregation of the $LaVO_3$-based secondary phase, a sharp discontinuity in the conductivity plot is observed at 950 °C for oxygen partial pressures below 10^{-15} atm, which is consistent with the third-stage reduction noted in Figure 7. Note that the expected conductivity of $LaVO_3$ would be orders of magnitude higher than the conductivity of the original $Sr_{0.02}La_{0.98}Nb_{0.7}V_{0.3}O_{4-\delta}$ phase.[38] In contrast, at lower temperatures, a plateau in conductivity is observed under reducing conditions. Commonly, such plateaus in conductivity behavior are related to regions where ionic species dominate the conductivity.

3.5. Conductivity in Wet/Dry Oxidizing Atmospheres. *3.5.1. Total Conductivity*. In wet inert atmospheres (e.g., wet N_2), one expects prevailing proton and oxygen vacancy contributions and a negligible *p*-type contribution (i.e., $K_{ox}{}^{1/2}p(O_2)^{1/4} \ll K^{1/2}[O]p(H_2O)^{1/2}$). Thus, the corresponding simplifications of eqs 20 and 22 yield

$$[OH_O^{\bullet}] = \frac{K[O]p(H_2O)}{4}\left[\left(1+\frac{8[Sr_{La}']}{K[O]p(H_2O)}\right)^{1/2}-1\right] \quad (27)$$

Otherwise, one may expect significant protonic and *p*-type electronic contributions, as given by eqs 21 and 22. This is demonstrated in Figures 11a and 11b, which compare the total (bulk + grain boundary) conductivity of $Sr_{0.02}La_{0.98}Nb_{0.7}V_{0.3}O_{4-\delta}$ and $Sr_{0.02}La_{0.98}NbO_{4-\delta}$ under nitrogen and oxygen in wet atmospheres ($p(H_2O) \approx 0.026$ atm) and dry atmospheres ($p(H_2O) \approx 1 \times 10^{-5}$ atm), respectively. Comparison between Figure 11a and Figure 11b reveals a much higher total conductivity under wet conditions than under dry conditions for both compositions, suggesting significant protonic contributions. The vanadium-free composition $Sr_{0.02}La_{0.98}NbO_{4-\delta}$ demonstrates a break in conductivity behavior at ~600 °C under both wet and dry conditions, corresponding to the fergusonite−scheelite phase transformation, in agreement with the behavior of similar acceptor-doped $LaNbO_4$ materials reported by Haugsrud et al.[2,3] In contrast, the vanadium-containing scheelite material, $Sr_{0.02}La_{0.98}Nb_{0.7}V_{0.3}O_{4-\delta}$, shows smooth increases in conductivity with increasing temperature, under both wet and dry conditions. Hence, the incorporation of vanadium, and the retention of the scheelite phase to room temperature, produces a material that offers a lower and more-stable activation energy for conduction across the entire temperature range. This characteristic allows the vanadium-containing material, $Sr_{0.02}La_{0.98}Nb_{0.7}V_{0.3}O_{4-\delta}$, to offer a higher total conductivity than the base composition, $Sr_{0.02}La_{0.98}NbO_{4-\delta}$, in the low-temperature range under wet conditions, despite a slightly lower conductivity at high temperatures. For both compositions, the total conductivity

(38) Cheng, Z.; Zha, S. W.; Aguiar, L.; Liu, M. L. *Solid State Ionics* **2005**, *176*, 1921.

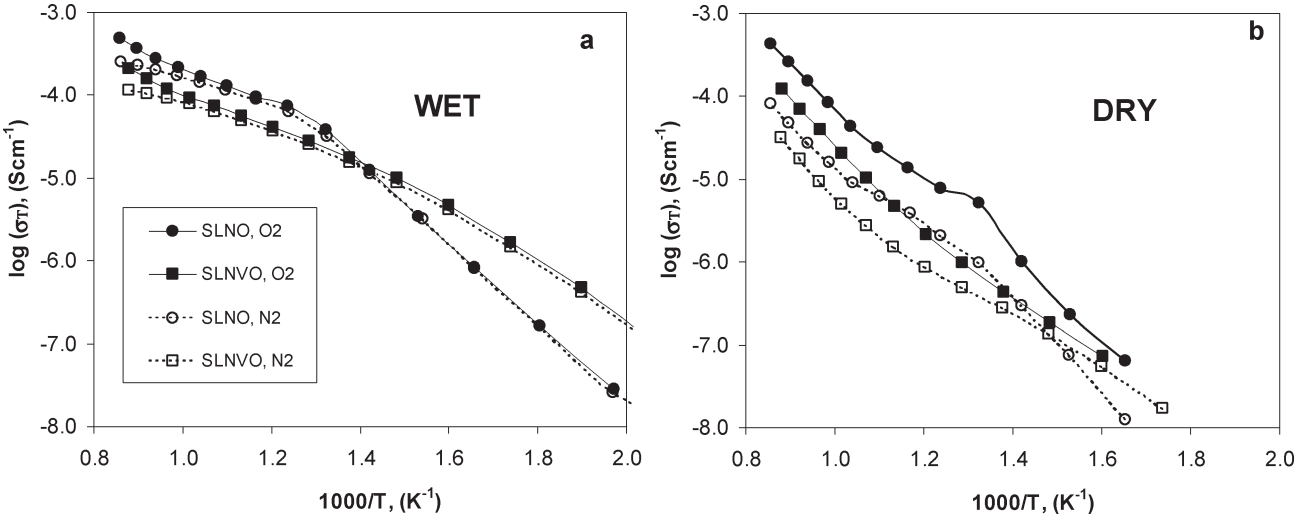

Figure 11. Total (bulk + grain boundary) conductivity of $Sr_{0.02}La_{0.98}Nb_{0.7}V_{0.3}O_{4-\delta}$ (SLNVO) and $Sr_{0.02}La_{0.98}NbO_{4-\delta}$ (SLNO) in nitrogen and oxygen for (a) wet atmospheres ($p(H_2O) \approx 0.026$ atm) and (b) dry atmospheres ($p(H_2O) \approx 1 \times 10^{-5}$ atm).

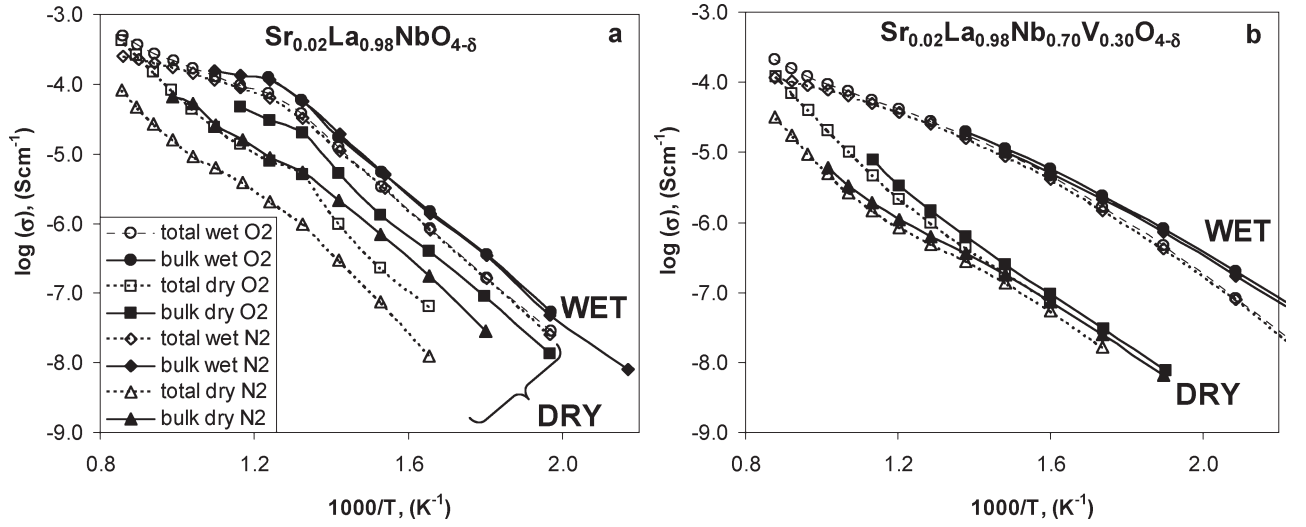

Figure 12. Total and bulk conductivities measured in wet ($p(H_2O) \approx 0.026$ atm) and dry ($p(H_2O) \approx 1 \times 10^{-5}$ atm) nitrogen and oxygen atmospheres for (a) $Sr_{0.02}La_{0.98}NbO_{4-\delta}$ materials and (b) $Sr_{0.02}La_{0.98}Nb_{0.7}V_{0.3}O_{4-\delta}$.

in wet nitrogen and oxygen atmospheres mirror each other up to high temperature, at which point the conductivity in oxygen exceeds that in nitrogen. This observation can be explained by considering the *p*-type electronic contribution of these materials that increases as the oxygen partial pressure increases (see Figure 10). Under dry conditions, the effect of the *p*-type conductivity is even more evident, with higher total conductivities measured in the more-oxidizing conditions, especially in the high-temperature range.

3.5.2. Bulk Transport. Figures 12a and 12b distinguish the bulk and total conductivities measured in nitrogen and oxygen for wet and dry atmospheres for $Sr_{0.02}La_{0.98}NbO_{4-\delta}$ and $Sr_{0.02}La_{0.98}Nb_{0.7}V_{0.3}O_{4-\delta}$ materials, respectively, based on fittings of impedance spectra. In general, both compositions show higher bulk conductivities than total conductivities, suggesting the existence of grain-boundary limitations to total conductivity. However, at higher temperatures under wet conditions, the total conductivity of both compositions becomes limited by the bulk transport (i.e., the grain-boundary conductivity begins to exceed the bulk). Note that this phenomenon occurs at lower onset temperatures in the case of $Sr_{0.02}La_{0.98}Nb_{0.7}V_{0.3}O_{4-\delta}$. Another interesting feature is the much higher bulk conductivity of $Sr_{0.02}La_{0.98}NbO_{4-\delta}$ than $Sr_{0.02}La_{0.98}Nb_{0.7}V_{0.3}O_{4-\delta}$ under dry conditions and its large dependence on oxygen partial pressure throughout the temperature range. This large decrease in conductivity when moving from a dry oxygen atmosphere to a nitrogen atmosphere suggests significant *p*-type electronic conductivity in $Sr_{0.02}La_{0.98}NbO_{4-\delta}$ for all temperatures. In contrast, $Sr_{0.02}La_{0.98}Nb_{0.7}V_{0.3}O_{4-\delta}$ exhibits this phenomenon only at the highest temperatures under dry conditions, whereas at lower temperatures, bulk conductivity becomes independent of atmosphere. Therefore, one can suggest a change from dominant *p*-type to ionic conductivity under dry conditions for $Sr_{0.02}La_{0.98}Nb_{0.7}V_{0.3}O_{4-\delta}$ with decreasing temperature, in agreement with Figure 10. Note that the lower *p*-type conductivity for

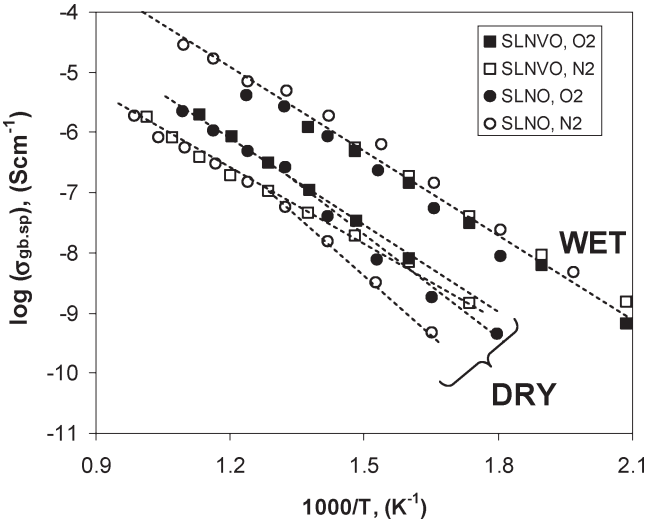

Figure 13. Specific grain-boundary conductivities of $Sr_{0.02}La_{0.98}Nb_{0.7}V_{0.3}O_{4-\delta}$ (SLNVO) and $Sr_{0.02}La_{0.98}NbO_{4-\delta}$ (SLNO) materials, measured in wet ($p(H_2O) \approx 0.026$ atm) and dry ($p(H_2O) \approx 1 \times 10^{-5}$ atm) nitrogen and oxygen atmospheres.

$Sr_{0.02}La_{0.98}Nb_{0.7}V_{0.3}O_{4-\delta}$, with respect to $Sr_{0.02}La_{0.98}NbO_{4-\delta}$, under dry oxidizing conditions, leads to a much more pronounced jump in conductivity upon hydration.

3.5.3. Specific Grain-Boundary Conductivity. The specific grain-boundary conductivities of $Sr_{0.02}La_{0.98}Nb_{0.7}V_{0.3}O_{4-\delta}$ and $Sr_{0.02}La_{0.98}NbO_{4-\delta}$, measured in various atmospheres, are plotted in Figure 13. The grain-boundary conductivities measured for all compositions are higher under wet conditions than under dry conditions, suggesting that the grain boundaries of these materials are proton-conducting. Moreover, the conductivity under wet conditions is similar for all compositions and oxygen partial pressures. This interesting feature implies a similar mechanism for proton transport in the grain boundary that is independent of vanadium content and bulk crystallographic structure (i.e., independent of the scheelite−fergusonite phase transition). In this respect, note that the activation energy for grain-boundary transport under wet conditions resembles that of bulk transport in the fergusonite phase (see Table 1). Under dry conditions, at high temperature, the specific grain-boundary conductivity is similar for both compositions and decreases upon reducing the oxygen partial pressure, which is characteristic of *p*-type electronic conductivity. The activation energy for grain-boundary conductivity in the scheelite material $Sr_{0.02}La_{0.98}Nb_{0.7}V_{0.3}O_{4-\delta}$ remains constant with temperature, whereas a notable break in the activation energy occurs for $Sr_{0.02}La_{0.98}NbO_{4-\delta}$ at temperatures corresponding to the scheelite−fergusonite phase transformation.

3.5.4. Proton and Total Ionic Conductivity. The proton and total ionic transport numbers of $Sr_{0.02}La_{0.98}Nb_{0.7}V_{0.3}O_{4-\delta}$ in an oxidizing wet atmosphere ($p(O_2) \approx 0.65$ atm) were separated using the EMF method. The partial proton and total ionic conductivities were calculated using the relation

$$\sigma_{\text{partial}} = t_i \sigma_T \quad (28)$$

where t_i represents the specific transference number and σ_T is the total conductivity measured in a wet oxygen atmosphere. Figure 14 compares the respective partial conductivities to the total conductivities measured in wet oxygen and nitrogen atmospheres. The proton conductivity corresponds closely to the total conductivity measured in nitrogen throughout the temperature range, whereas the total conductivity measured in oxygen surpasses that of the proton conduction at elevated temperatures. This indicates an increasing electronic contribution to total conductivity under more-oxidizing conditions at the highest temperatures, in agreement with Figure 10. In contrast, the material becomes a pure proton conductor in both atmospheres at lower temperatures. The curvature of proton conductivity at the highest temperatures may be related to the commencement of dehydration. The total ionic conductivity equals that of the proton conductivity, within experimental error, suggesting negligible oxide-ion conduction in this material under wet conditions throughout the studied temperature range.

Table 1. Activation Energy for Bulk and Grain-Boundary Conductivity in $Sr_{0.02}La_{0.98}NbO_{4-\delta}$ (SLNO) and $Sr_{0.02}La_{0.98}Nb_{0.7}V_{0.3}O_{4-\delta}$ (SLNVO) Materials under Wet Conditions, Calculated for Temperatures below That of the Fergusonite−Scheelite Phase Transformation

		Activation Energy (kJ/mol)	
conductivity type	atmosphere	SLNVO composition	SLNO composition
bulk	O_2	67.5 ± 2	92.7 ± 6
bulk	N_2	64.1 ± 2	91.7 ± 3
grain-boundary	O_2	93.2 ± 2	92.2 ± 5
grain-boundary	N_2	86.1 ± 3	94.2 ± 2

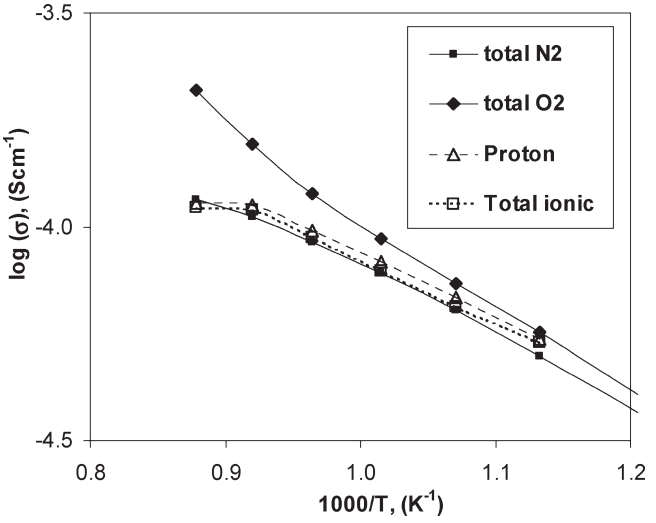

Figure 14. Comparison of partial proton and total ionic conductivities of $Sr_{0.02}La_{0.98}Nb_{0.7}V_{0.3}O_{4-\delta}$ measured under oxidizing conditions ($p(O_2) = 0.65$ atm) to the total conductivities measured under wet ($p(H_2O) \approx 0.026$ atm) oxygen and nitrogen atmospheres.

Conclusions

The high-temperature scheelite phase of $Sr_{0.02}La_{0.98}Nb_{1-x}V_xO_{4-\delta}$ materials can be stabilized to room temperature by vanadium substitution in the compositional range of $0.25 \leq x \leq 0.325$. Such stabilization allows the composition $Sr_{0.02}La_{0.98}Nb_{0.7}V_{0.3}O_{4-\delta}$ to (i) maintain a constant thermal expansion coefficient (TEC) throughout the temperature range and (ii) offer pure proton conduction of higher conductivity than the base composition

$Sr_{0.02}La_{0.98}NbO_{4-\delta}$ in the low-temperature range, under wet oxidizing conditions. A wide ionic domain is observed that increases as the temperature decreases. Use of this electrolyte in biogas-imitating mixtures is shown to not cause decomposition at temperatures approaching 600 °C. At higher temperatures, a sharp discontinuity in conduction is observed, corresponding to partial decomposition and segregation of a $LaVO_3$-based secondary phase, in coexistence with the scheelite phase. Nevertheless, in a fuel cell scenario, phase stability may be extended, because of an oxygen partial pressure gradient with the oxidizing conditions of the cathode. Generally, both $Sr_{0.02}La_{0.98}Nb_{0.7}V_{0.3}O_{4-\delta}$ and $Sr_{0.02}La_{0.98}NbO_{4-\delta}$ compositions show higher bulk conductivities than total conductivities, because of grain-boundary limitations to total conductivity. However, at higher temperatures, under wet conditions, the total conductivity of both compositions becomes limited by the bulk. Under dry oxidizing conditions, the *p*-type conductivity for $Sr_{0.02}La_{0.98}NbO_{4-\delta}$ is shown to be higher than that of $Sr_{0.02}La_{0.98}Nb_{0.7}V_{0.3}O_{4-\delta}$. The grain boundaries of these materials also conduct protons, and the conductivity under wet conditions is independent of composition and oxygen partial pressure. This implies a similar mechanism for proton transport in the grain boundary, which is independent of vanadium content and the bulk scheelite−fergusonite phase transition. Under wet conditions, $Sr_{0.02}La_{0.98}Nb_{0.7}V_{0.3}O_{4-\delta}$ is found to be a pure proton conductor in oxygen and argon atmospheres at temperatures lower than ~700 °C. The total ionic conductivity equals that of the proton conductivity, within experimental error, suggesting negligible oxide-ion conduction in this material, under these conditions.

Acknowledgment. This work was supported by the FCT, Portugal (through Grant Nos. PTDC/CTM/64357/2006, FCT, SFRH/BD/60265/2009, FCT, PTDC/CTM/105424/2008, PTDC/CTM/100412/2008).